

文章编号:1673-8926(2020)04-0172-09

DOI:10.12108/yxyqc.20200418

引用:崔永正,姜瑞忠,郜益华,等.空间变导流能力压裂井 CO₂ 驱试井分析.岩性油气藏,2020,32(4):172-180.

Cite:CUI Y Z,JIANG R Z,GAO Y H,et al. Pressure transient analysis of hydraulic fractured vertical wells with variable conductivity for CO₂ flooding. Lithologic Reservoirs,2020,32(4):172-180.

空间变导流能力压裂井 CO₂ 驱试井分析

崔永正¹,姜瑞忠¹,郜益华²,乔欣³,王琼¹

(1. 中国石油大学(华东)石油工程学院,山东青岛 266580; 2. 中海油研究总院有限责任公司,北京 100028; 3. 中国石油北京油气调控中心,北京 100007)

摘要:目前利用压裂井进行 CO₂ 驱已成为低渗透油藏开发的主要技术之一,水力裂缝导流能力是决定开发效果的关键因素,而试井研究多采用与实际不符的恒定缝宽假设对水力裂缝进行描述。基于三区复合理论,建立考虑空间变导流能力压裂直井的 CO₂ 驱试井模型,通过 Laplace 变换进行求解,进行数值反演,绘制典型试井曲线。典型曲线可分为井筒储集段、井筒储集后过渡段、双线性流段、地层线性流段、第一径向流段、第一过渡流段、第二径向流段、第二过渡流段、第三径向流段共 9 个阶段。对模型影响因素进行分析,裂缝导流能力越大,双线性流段阶段压差越小,CO₂ 越容易注入;考虑裂缝导流能力变化后,早期压差增大,压力及压力导数曲线都呈现一定的上升,表现出类似表皮系数增大的现象;CO₂ 及过渡区半径主要对径向流的持续时间及过渡流出现时间产生影响,半径越大,对应过渡流出现的时间越晚;一区与二区流度比越大,过渡区及最外区流动阶段所消耗的压差越大;二区与三区流度比,最外区流动阶段所消耗的压差越大。

关键词:压裂直井;空间变导流能力;CO₂ 驱;试井分析

中图分类号:TE348

文献标志码:A

Pressure transient analysis of hydraulic fractured vertical wells with variable conductivity for CO₂ flooding

CUI Yongzheng¹, JIANG Ruizhong¹, GAO Yihua², QIAO Xin³, WANG Qiong¹

(1. College of Petroleum Engineering, China University of Petroleum (East China), Qingdao 266580, Shandong, China;

2. CNOOC Research Institute Co., Ltd., Beijing 100028, China; 3. PetroChina Oil & Gas Pipeline Control Center, Beijing 100007, China)

Abstract: At present, CO₂ flooding with hydraulic fractured vertical wells has become one of the main technologies for the development of low permeability reservoirs. Hydraulic fracture conductivity is a key factor influencing the production performance of fractured wells, and now most well test models were based on the assumption of a constant fracture width, failing to simulate the space variable width of hydraulic fractures. Based on three-zone composite theory, a CO₂ flooding well test model of hydraulic fractured vertical wells considering with variable

收稿日期:2019-05-20;修回日期:2019-09-04;网络发表日期:2019-12-11

基金项目:国家重大科技专项“厚层非均质气藏产能评价及预测技术”(编号:2016ZX05027-004-004)和“低渗、特低渗油藏水驱扩大波及体积方法与关键技术”(编号:2017ZX05013-002)联合资助

作者简介:崔永正(1992—),男,中国石油大学(华东)在读博士研究生,研究方向为油气藏数值模拟及动态分析。地址:(266580)山东省青岛市黄岛区长江西路 66 号中国石油大学(华东)石油工程学院。Email:986012825@qq.com

通信简介:姜瑞忠(1964—),男,博士,教授,博士生导师,主要从事油气田开发方面的教学和研究工作。Email:jrzong@126.com。

conductivity was established, and the Laplace transformation was adopted to solve this model, and then the numerical inversion was carried out to draw typical well test curve. According to the pressure response characteristics, the pressure transient type curve was divided into nine stages including wellbore storage stage, skin effect stage, bilinear flow stage, linear flow stage, the first radial flow stage, the first transition stage, the second radial flow stage, the second transition stage and the late radial flow. Sensitivity analysis was carried out to investigate the influence of several factors on pressure transient. The results show that the larger the fracture conductivity was, the smaller the pressure of the bilinear flow stage was, and the easier CO₂ can be injected. When the space variable conductivity was considered, the pressure of early flow stages increased, and the pressure and pressure derivative curve of early flow stages rised which was similar to the effect of a larger skin factor. The radius of region-1 and region-2 mainly had an influence on the starting time of transition stage and the duration of radial flow. When the radius of region-1 and region-2 was larger, the start time of the transfer stage was prolonged. When M_{12} was enhanced, the pressure of the flow in both region-2 and region-3 was larger. When M_{23} was enhanced, the pressure of the flow in region-3 elevated.

Key words: hydraulic fractured vertical wells; space variable conductivity; CO₂ flooding; pressure transient analysis

0 引言

在我国,低渗透油藏具有分布广,储量大,开发潜力大等特征^[1-2],低渗透油田的高效开发利用对确保我国油气可持续发展具有重要战略意义。针对低渗透油田渗透率低,水驱开发效果差的特点,压裂井与 CO₂ 驱结合的开发方式引起了国内外学者的关注^[3-4]。

试井作为了解地下油藏和流体性质的重要手段,国内外许多学者针对 CO₂ 驱试井解释数学模型进行了大量的研究。Tang 等^[5]建立了基本的三区复合油藏模型;Su 等^[6]、阎燕等^[7]、李友全等^[8]、苏玉亮等^[9]研究了考虑应力敏感的 CO₂ 驱直井的三区复合模型,并对各因素进行了敏感性分析;Li 等^[10-11]开展了基于组分模型的 CO₂ 驱直井及多段井试井研究,对试井曲线及各组分在地层中的分布情况进行了分析;姜瑞忠等^[12]建立了基于水平井的 CO₂ 驱三区复合试井模型,将典型曲线分为 9 个阶段,并对各因素进行了敏感性分析。

压裂井试井作为近年来研究的热点,Teng 等^[13]、Guo 等^[14]、姬靖皓等^[15]、Jia 等^[16]针对压裂井试井模型进行的大量研究都是以恒定裂缝宽度作为假设,但实际上支撑裂缝宽度从缝端到缝口逐渐变化,恒定缝宽模型假设与实际不符。针对变导流能力裂缝,国内外学者进行了相关研究,郭建春等^[17]建立了基于楔形缝的压裂直井产量预测模型,表明楔形缝产量预测模型能够以更真实的裂缝形态来预测压后产量;孙贺东等^[18]利用混合有限元方法对变导流能力多级压裂水平井现代产量递减进行了分析,发现裂缝变导流能力主要对产量递减曲线产期产生影响;高阳等^[19]建立了考虑变导流能力的多级压

裂水平井试井模型,并提出了变导流能力裂缝的处理方法;Luo 等^[20]建立了变导流能力压裂直井的试井分析模型;Huang 等^[21]建立了考虑裂缝部分闭合的压裂直井试井模型;Liu 等^[22]建立了考虑复杂裂缝形态及变导流能力的试井模型;Liu 等^[23]建立了三层油藏考虑变导流能力压裂直井的解析解,并进行了求解和敏感性分析。综上所述,目前尚没有考虑裂缝空间变导流能力的 CO₂ 驱试井模型。

因此,在前人研究的基础上,建立低渗透油藏空间变导流垂直裂缝井 CO₂ 驱试井解释模型,利用 Laplace 变换等数学方法获得拉氏空间解析解,利用 Stehfest 数值反演绘制典型特征曲线并进行影响因素分析。

1 模型的建立与求解

1.1 物理模型

根据 CO₂ 驱油过程中油藏流体的不同性质,基于三区复合模型渗流理论,物理模型如图 1 所示。内

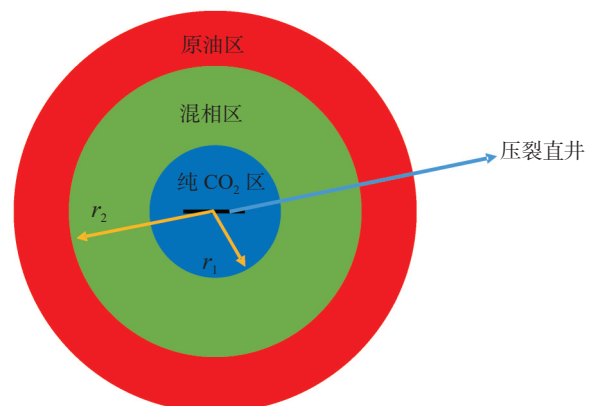


图 1 CO₂ 驱油三区复合物理模型
Fig. 1 Physical modeling of three-zone composite vertical fractured wells for CO₂ flooding

区充满 CO_2 , 表现为 CO_2 气相单相渗流, 半径为 r_1 ; 过渡区为在混溶/不混溶条件下 CO_2 与原油的混合区, 半径为 r_2 ; 外区为单相储层原油区。该复合模型的假设条件包括: ①油气藏中油气共存; ②流体渗流过程中温度恒定, 且遵循达西渗流原理; ③储层为水平、均质、等厚和无限大, 初始压力处处相等; ④裂缝半长为 X_f , 裂缝的宽度不等, 为空间变导流能力; ⑤忽略重力与毛管压力的影响;

1.2 数学模型

1.2.1 储层渗流数学模型

根据上述三区复合模型的假设, 对各区质量守恒方程和综合方程进行推导。

(1) 内区

内区为纯 CO_2 区, 为气相单相渗流, 其质量守恒方程为

$$\frac{1}{r} \frac{\partial}{\partial r} \left[k r \left(\frac{K_{rg}}{\mu_g} \rho_g \right) \frac{\partial p_1}{\partial r} \right] = \Phi \frac{\partial (S_g \rho_g)}{\partial t} \quad (1)$$

式中: r 为油藏半径, m; k 油藏渗透率, mD; K_{rg} 为气相相对渗透率; μ_g 为气相有效黏度, Pa·s; ρ_g 为气相密度, kg/m^3 ; S_g 为气相的饱和度; Φ 为孔隙度; p_1 为 CO_2 区地层压力, Pa。

式(1)可进一步化简为

$$\frac{1}{r} \frac{\partial}{\partial r} \left[k r \left(\frac{K_{rg}}{\mu_g} \rho_g \right) \frac{\partial p_1}{\partial r} \right] = \Phi S_g \frac{\partial \rho_g}{\partial p} \frac{\partial p}{\partial t} \quad (2)$$

其中:

$$C_g = \frac{\partial V_g}{\partial p} \frac{1}{V_g} = \frac{\partial (V_g/m)}{\partial p} \frac{m}{V_g} = \frac{\partial (1/\rho_g)}{\partial p} \rho_g = \frac{\partial \rho_g}{\partial p} \frac{1}{\rho_g} \quad (3)$$

式中: C_g 为气体压缩系数, $1/\text{Pa}$; V_g 为气相体积, m^3 。

式(2)可进一步化简为

$$\frac{1}{r} \frac{\partial}{\partial r} \left[k r \left(\frac{K_{rg}}{\mu_g} \rho_g \right) \frac{\partial p_1}{\partial r} \right] = \Phi S_g \rho_g C_g \frac{\partial p}{\partial t} \quad (4)$$

上述方程为非线性方程, 引入拟压力对上述方程进行线性化

$$m_1(p) = 2 \int_{p_0}^{p_1} \left(\frac{K_{rg}}{\mu_g} \rho_g \right) dp \quad (5)$$

$$m_2(p) = 2 \int_{p_0}^{p_2} \left(\frac{K_{rg}}{\mu_g} \rho_g + \frac{K_{ro}}{\mu_o} \rho_o \right) dp \quad (6)$$

$$m_3(p) = 2 \int_{p_0}^{p_3} \left(\frac{K_{ro}}{\mu_o} \rho_o \right) dp \quad (7)$$

式中: p_0 为参考压力, Pa; p_2 为过渡区地层压力, Pa; p_3 为原油区地层压力, Pa。

引入式(2), 对上式进行线性化, 得

$$\frac{1}{r} \frac{\partial}{\partial r} \left(r \frac{\partial \psi_1}{\partial r} \right) = \frac{\Phi S_g \rho_g C_g \mu_g}{k K_{rg}} \frac{\partial \psi_1}{\partial t} = \frac{1}{\eta_1} \frac{\partial \psi_1}{\partial t} \quad (8)$$

利用表1中无因次量, 对上述数学模型进行无因次化, 并进行 Laplace 变换, 内区综合方程为

$$\frac{\partial^2 \bar{\psi}_{1D}}{\partial r_D^2} + \frac{1}{r_D} \frac{\partial \bar{\psi}_{1D}}{\partial r_D} - f_1 \bar{\psi}_{1D} = 0 \quad (9)$$

式中: $f_1 = u$; u 为 Laplace 变量。

(2) 中间区

中间区为 CO_2 与原油的混合区, 其质量守恒方程为

$$\frac{1}{r} \frac{\partial}{\partial r} \left[k r \left(\frac{K_{rg}}{\mu_g} \rho_g + \frac{K_{ro}}{\mu_o} \rho_o \right) \right] \frac{\partial p_2}{\partial r} = \Phi \frac{\partial (S_g \rho_g + S_o \rho_o)}{\partial t} \quad (10)$$

式中: K_{ro} 为油相相对渗透率; μ_o 为油相有效黏度, Pa·s; ρ_o 为油相密度, kg/m^3 ; S_o 为气相的饱和度。

利用式(6)中拟压力对上式(10)进行线性化, 利用表1无因次量, 对上述数学模型进行无因次化, 进行 Laplace 变换, 中间区综合方程为:

$$\frac{\partial^2 \bar{\psi}_{2D}}{\partial r_D^2} + \frac{1}{r_D} \frac{\partial \bar{\psi}_{2D}}{\partial r_D} - f_2 \bar{\psi}_{2D} = 0 \quad (11)$$

式中: $f_2 = \omega_{12} u_o$ 。

(3) 外区

外区为单相原油区, 原油单相流动, 其质量守恒方程为

$$\frac{1}{r} \frac{\partial}{\partial r} \left[k r \left(\frac{K_{ro}}{\mu_o} \rho_o \right) \right] \frac{\partial p_3}{\partial r} = \Phi \frac{\partial (S_{oi} \rho_o)}{\partial t} \quad (12)$$

式中: S_{oi} 为原始含油饱和度。

利用式(7)对式(12)进行线性化, 利用表1无因次量, 对上述数学模型进行无因次化, 进行 Laplace 变换, 外区综合方程为

$$\frac{\partial^2 \bar{\psi}_{3D}}{\partial r_D^2} + \frac{1}{r_D} \frac{\partial \bar{\psi}_{3D}}{\partial r_D} - f_3 \bar{\psi}_{3D} = 0 \quad (13)$$

式中: $f_3 = \omega_{13} u_o$ 。

(4) 边界条件

外边界条件为

$$\lim_{r_D \rightarrow \infty} \bar{\psi}_{3D} = 0 \quad (14)$$

线源内边界条件为

$$r_D \frac{\partial \bar{\psi}_{1D}}{\partial r_D} \Big|_{r_D=0} = -\frac{\hat{q}}{q_i} \quad (15)$$

式中: \hat{q} 为线源流量, kg/s 。

一区与二区交界面条件

$$\begin{cases} \bar{\psi}_{1D} = \bar{\psi}_{2D}(r_D = r_{1D}) \\ \frac{\partial \bar{\psi}_{1D}}{\partial r_D} = \frac{1}{M_{12}} \frac{\partial \bar{\psi}_{2D}}{\partial r_D}(r_D = r_{1D}) \end{cases} \quad (16)$$

二区与三区交界面条件

$$\begin{cases} \bar{\psi}_{2D} = \bar{\psi}_{3D}(r_D = r_{2D}) \\ \frac{\partial \bar{\psi}_{2D}}{\partial r_D} = \frac{1}{M_{23}} \frac{\partial \bar{\psi}_{3D}}{\partial r_D}(r_D = r_{2D}) \end{cases} \quad (17)$$

对式(9)、式(11)、式(13)及边界条件进行联立求解,可以得到 CO₂ 驱内区线源所引起的压力响应为

$$\bar{\psi}_{1D} = \frac{\hat{q}}{q_i} \left[K_0(\sqrt{f_1} r_D) + A_c I_0(\sqrt{f_1} r_D) \right] \quad (18)$$

式中: $g_1 = \frac{a_{31} a_{44} - a_{34} a_{41}}{a_{34} a_{42} - a_{32} a_{44}}$, $a_{11} = I_0(\sqrt{f_1} r_{1D})$, $a_{12} = I_0(\sqrt{f_1} r_{1D})$, $a_{13} = I_0(\sqrt{f_2} r_{1D})$, $a_{14} = K_0(\sqrt{f_2} r_{1D})$, $a_{21} = I_1(\sqrt{f_1} r_{1D})$, $a_{12} = -K_1(\sqrt{f_1} r_{1D})$, $a_{23} = \frac{\sqrt{f_2}}{M_{12} \sqrt{f_1}} I_1(\sqrt{f_2} r_{1D})$, $a_{24} = -\frac{\sqrt{f_2}}{M_{12} \sqrt{f_1}} K_1(\sqrt{f_2} r_{1D})$, $a_{31} = I_0(\sqrt{f_2} r_{2D})$, $a_{32} = K_0(\sqrt{f_2} r_{2D})$, $a_{33} = K_0(\sqrt{f_3} r_{2D})$, $a_{34} = K_0(\sqrt{f_3} r_{2D})$, $a_{41} = I_1(\sqrt{f_2} r_{2D})$, $a_{42} = -K_1(\sqrt{f_2} r_{2D})$, $a_{43} = \frac{\sqrt{f_3}}{M_{23} \sqrt{f_1}} I_1(\sqrt{f_3} r_{2D})$, $a_{44} = -\frac{\sqrt{f_3}}{M_{23} \sqrt{f_2}} K_1(\sqrt{f_3} r_{2D})$ 。

表 1 无量纲量

Table 1 Definitions of the dimensionless variables

无量纲变量	定义	无量纲变量	定义
无量纲半径	$r_D = \frac{r}{x_F}$	无量纲空间坐标	$x_D = \frac{x}{x_F}, y_D = \frac{y}{x_F}$
无量纲时间	$t_D = \frac{t}{x_F^2} \eta_1$	无量纲拟压力	$\psi_{jD} = \frac{\pi k h [m_j(p_0) - m_j(p_j)]}{q_i} \quad (j = 1, 2, 3)$ $q_i = q_o \rho_o + q_g \rho_g$
无量纲井储系数	$C_D = \frac{C}{2 \pi \varphi_1 C_{11} h x_F^2}$	CO ₂ 区与过渡区流度比	$M_{12} = \frac{\left(\frac{K_{rg}}{\mu_g}\right)_1}{\left(\frac{K_{ro}}{\mu_o} + \frac{K_{ro}}{\mu_o}\right)_2}$
过渡区与原油区流度比	$M_{23} = \frac{\left(\frac{K_{rg}}{\mu_g} + \frac{K_{ro}}{\mu_o}\right)_2}{\left(\frac{K_{ro}}{\mu_o}\right)_3}$	CO ₂ 区与过渡区导压系数比	$\omega_{12} = \frac{\eta_1}{\eta_2}$
CO ₂ 区与原油区导压系数比	$\omega_{13} = \frac{\eta_1}{\eta_3}$	无量纲裂缝宽度	$w_{FD} = \frac{w_F}{x_F}$
无量纲导流能力	$R_{FD} = \frac{K_F w_F}{k x_F}$	CO ₂ 区导压系数	$\eta_1 = \frac{k K_{rg}}{\Phi C_g S_g \mu_g}$
过渡区导压系数	$\eta_2 = \frac{k}{\Phi} \frac{\frac{K_{rg}}{\mu_g} \rho_g + \frac{K_{ro}}{\mu_o} \rho_o}{C_i + (\rho_o - \rho_g) \frac{\partial S_o}{\partial p}}$ $C_i = C_o S_o \rho_o + C_g S_g \rho_g$	原油区导压系数	$\eta_3 = \frac{k K_{ro}}{\Phi C_o \mu_o S_o}$
单位长度裂缝流量	$q_{LD} = \frac{x_F q_L}{q_i}$	裂缝无量纲流量	$q_{FD} = \frac{q_F}{q_i}$
内区半径	$r_{1D} = \frac{r_1}{x_F}$	过渡区半径	$r_{2D} = \frac{r_2}{x_F}$

1.2.2 有限导流能力压裂直井方程
水力裂缝孔隙体积很小,忽略孔隙体积变化的

影响,裂缝渗流满足达西定律,可得压裂裂缝中质量守恒方程为:

$$\frac{\partial}{\partial x} \left(\frac{K_F K_{rg} \rho_g}{\mu_g} \frac{\partial p_F}{\partial x} \right) + \frac{\partial}{\partial y} \left(\frac{K_F \rho_g K_{rg}}{\mu_g} \frac{\partial p_F}{\partial y} \right) = 0 \quad (19)$$

式中: K_F 为水力裂缝渗透率, mD; p_F 为水力裂缝压力, Pa。

由于水力压裂形成的裂缝宽度解一般较小, 故在式(19)左端第2项取积分平均处理, 从而可得到

$$\frac{\partial}{\partial y} \left(\frac{K_F \rho_g K_{rg}}{\mu_g} \frac{\partial p_F}{\partial y} \right) = \frac{2}{w_F} \left[\frac{K_F \rho_g K_{rg}}{\mu_g} \frac{\partial p_F}{\partial y} \right]_{y=\frac{w_F}{2}} - \left[\frac{K_F \rho_g K_{rg}}{\mu_g} \frac{\partial p_F}{\partial y} \right]_{y=0} \quad (20)$$

式中: w_F 为裂缝宽度, m。

单位裂缝长度流量可表示为

$$q_L = 2h \frac{k K_{rg} \rho_g}{\mu_g} \frac{\partial p_L}{\partial y} \bigg|_{y=\frac{w_F}{2}} \quad (21)$$

式中: h 为地层厚度, m; q_L 为水力裂缝单位长度流量, $\text{kg}/(\text{m} \cdot \text{s})$ 。

从水力裂缝右翼流入井筒的产量为

$$q_F = w_F h \frac{K_F K_{rg} \rho_g}{\mu_g} \frac{\partial p_F}{\partial x} \bigg|_{x=0} \quad (22)$$

式中: q_F 为水力裂缝右翼流入井的产量, kg/s 。

对式(20)、式(21)、式(22)进行线性化, 利用表1无因次量进行无因次化, 并进行 Laplace 变换, 可得压裂直井综合方程。其中有限导流裂缝内流动方程:

$$\frac{\partial}{\partial x_D} \left(R_{FD} \frac{\partial \bar{\psi}_{FD}}{\partial x_D} \right) + 2 \frac{\partial \bar{\psi}_{1D}}{\partial y_D} \bigg|_{y_D=\frac{w_{FD}}{2}} = 0 \quad (23)$$

定产内边条件

$$\frac{\partial \bar{\psi}_{FD}}{\partial x_D} \bigg|_{x_D=0} = - \left(\frac{2\pi}{R_{FD}} \bar{q}_{FD} \right) \bigg|_{x_D=0} \quad (24)$$

裂缝与储层交界面条件

$$\frac{\partial \bar{\psi}_{1D}}{\partial y_D} \bigg|_{x_D=\frac{w_D}{2}} = -\pi \bar{q}_{LD} \quad (25)$$

裂缝根段封闭条件

$$\frac{\partial^2 \bar{\psi}_{FD}}{\partial x_D^2} \bigg|_{x_D=1} = 0 \quad (26)$$

1.3 数学模型求解

对于压裂井而言, 人工裂缝是油气的主要流动通道, 裂缝的物理模型对计算结果有重要影响。在

裂缝闭合后, 裂缝宽度不是恒定的, 靠近裂缝端部的铺砂浓度较小, 靠近井眼部分的裂缝铺砂浓度较高, 最终形成的支撑裂缝宽度从缝端到缝口逐渐变宽, 如图2所示, 裂缝导流能力随裂缝长度而减小, 假设计算公式^[18]为

$$R_{FD} = R_{FD0} \left[1 - b_s \ln(1 + x_{FD}) \right] \quad (27)$$

式中: R_{FD0} 为缝口处裂缝无因次导流能力, m^3 ; b_s 空间变导流能力系数; x_F 为水力裂缝半长, m。

利用高阳等^[19]提出的方法对变导流能力裂缝进行处理, 将无因次水力裂缝半长等分成 n 份, 步长 Δx_D , \bar{x}_{Dj} 为第 j 个裂缝单元格的中点, x_{Dj} 为第 j 个离散端点, 如下图2所示, 当离散单元无限小时, 假设每个离散单元内流量均匀分布。

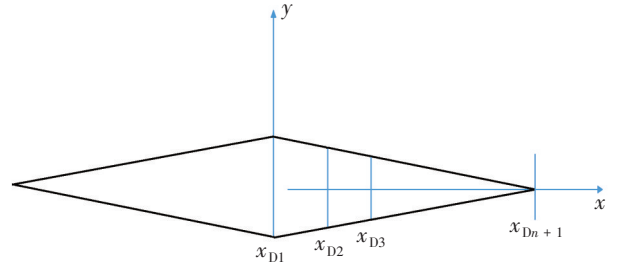


图2 水力裂缝划分示意图

Fig. 2 Schematic of discretization of the hydraulic fracture

从水力裂缝示意图中, 可得裂缝离散单元端点和中点表达式为

$$\begin{cases} x_{Dj} = (j-1) \Delta x_D \\ \bar{x}_{Dj} = \left(j - \frac{1}{2} \right) \Delta x_D \end{cases} \quad (28)$$

将式(25)代入式(23)中, 可得

$$\frac{\partial}{\partial x_D} \left(R_{FD} \frac{\partial \bar{\psi}_{FD}}{\partial x_D} \right) = 2\pi \bar{q}_{LD} \quad (29)$$

对两侧同时进行积分, 得:

$$\int_0^{x_D} \frac{\partial}{\partial x_D} \left(R_{FD} \frac{\partial \bar{\psi}_{FD}}{\partial x_D} \right) dx_D = \int_0^{x_D} 2\pi \bar{q}_{LD} dx_D \quad (30)$$

将边界条件式(24)代入式(30), 化简可得

$$R_{FD} \frac{\partial \bar{\psi}_{FD}}{\partial x_D} + 2\pi \bar{q}_{FD} = \int_0^{x_D} 2\pi \bar{q}_{LD} dx_D \quad (31)$$

对式(31)两侧同时进行积分, 得

$$\int_0^{x_D} R_{FD} \frac{\partial \bar{\psi}_{FD}}{\partial x_D} dx_D + \int_0^{x_D} 2\pi \bar{q}_{FD} dx_D = \int_0^{x_D} \int_0^{x_D} 2\pi \bar{q}_{LD} dx_D dx_D \quad (32)$$

式(32)可进一步化简为

$$\int_0^{x_D} R_{FD} d\bar{\psi}_{FD} + 2\pi x_D \bar{q}_{FD} = 2\pi x_D \int_0^{x_D} \bar{q}_{LD} dx_D - 2\pi \int_0^{x_D} x_D \bar{q}_{LD} dx_D \quad (33)$$

水力裂缝半长等分成 n 份,则第 i 段裂缝的压力降为

$$\sum_{j=1}^i R_{FDj} \int_{x_{Dj}}^{x_{Dj+1}} d\bar{\psi}_{FD} + 2\pi x_{Di} \bar{q}_{FD} = 2\pi x_{Di} \sum_{j=1}^i \bar{q}_{LDj} \int_{x_{Dj}}^{x_{Dj+1}} dx_D + 2\pi \sum_{j=1}^i \bar{q}_{LDj} x_{Dj} \int_{x_{Dj}}^{x_{Dj+1}} dx_D \quad (34)$$

式(34)可进一步化简为

$$\sum_{j=1}^i R_{FDj} [\bar{\psi}_{FD}(x_{Dj+1}) - \bar{\psi}_{FD}(x_{Dj+1})] + 2\pi x_D \bar{q}_{FD} = 2\pi x_{Di} \Delta x_D \sum_{j=1}^i \bar{q}_{LDj} + 2\pi \Delta x_D \sum_{j=1}^i \bar{q}_{LDj} x_{Dj} \quad (35)$$

当 $i = 1$ 时,对式(34)进行化简,可得

$$\bar{\psi}_{FD1} = \bar{\psi}_{wD} - \frac{2\pi x_{D1} \bar{q}_{FD}}{R_{FD1}} \quad (36)$$

当 $i = 2$ 时,对式(34)进行化简,可得

$$\bar{\psi}_{FD2} = \bar{\psi}_{wD} + 2\pi \Delta x_D^2 \frac{\bar{q}_{LD}(x_{D1})}{R_{FD2}} - 2\pi \bar{q}_{FD} \left(\frac{1}{R_{FD1}} - \frac{1}{R_{FD2}} \right) - \frac{2\pi x_{D2} \bar{q}_{FD}}{R_{FD2}} \quad (37)$$

当 $i = 3$ 时,对式(34)进行化简,可得

$$\begin{aligned} \bar{\psi}_{FD3} = & \bar{\psi}_{wD} - 2\pi x_{D1} \bar{q}_{FD} \left(\frac{1}{R_{FD1}} - \frac{1}{R_{FD2}} \right) - \\ & 2\pi x_{D2} \bar{q}_{FD} \left(\frac{1}{R_{FD2}} - \frac{1}{R_{FD3}} \right) - \frac{2\pi x_{D3} \bar{q}_{FD}}{R_{FD3}} + \\ & 2\pi \Delta x_D^2 \bar{q}_{LD}(x_{D1}) \left(\frac{1}{R_{FD2}} + \frac{1}{R_{FD3}} \right) + \\ & 2\pi \Delta x_D^2 \frac{\bar{q}_{LD}(x_{D2})}{R_{FD3}} \end{aligned} \quad (38)$$

则第 i 段裂缝的压力解为

$$\begin{aligned} \bar{\psi}_{FDi} = & \bar{\psi}_{wD} + 2\pi \Delta x_D^2 \sum_{j=1}^{i-2} \left[\bar{q}_{LD}(x_{Dj}) \sum_{n=j+1}^i \frac{1}{R_{FDn}} \right] + \\ & 2\pi \Delta x_D^2 \frac{\bar{q}_{LD}(x_{Di-1})}{R_{FDi}} - 2\pi \bar{q}_{FD} \cdot \\ & \sum_{j=1}^{i-1} x_{Dj} \left(\frac{1}{R_{FDj}} + \frac{1}{R_{FDj+1}} \right) - \frac{2\pi x_{Di} \bar{q}_{FD}}{R_{FDi}} \end{aligned} \quad (39)$$

由式(18)可得,第 i 段裂缝所产生的压力相应为

$$\bar{\psi}_{FDi} = \int_{x_{Di}}^{x_{Di+1}} \bar{q}_{LD} \left[K_0(\sqrt{f_1} r_D) + A_c I_0(\sqrt{f_1} r_D) \right] dx_D \quad (40)$$

裂缝内流体总量等于各裂缝段流量之和

$$\bar{q}_{FD} = \sum_{i=1}^n \Delta x_D \bar{q}_{LDi} \quad (41)$$

联合式(39)、式(40)、式(41),可得到 $n + 1$ 个线性方程,对应 $n + 1$ 个未知数。对方程组进行求解,利用杜哈美原理考虑井筒储集效应和表皮因子的影响,得到如下无因次井底压力

$$\bar{\psi}_{wDH} = \frac{u \bar{\psi}_{wD} + S}{u + u^2 C_D (u \bar{\psi}_{wD} + S)} \quad (42)$$

2 特征曲线分析

根据上述模型推导,编制程序计算压力及压力导数曲线,绘制有限导流能力裂缝 CO₂ 驱三区复合油藏典型试井曲线。相关参数及具体流态划分如图 3 所示,其典型试井曲线可分为以下 9 个阶段:①井筒储集阶段,压力及压力导数曲线斜率均为 1;②井筒储集后过渡阶段;③双线性流阶段,此时地层及水力裂缝都存在线性流,拟压力曲线及拟压力导数曲线为斜率为“1/4”的平行直线;④地层线性流阶段,拟压力曲线及拟压力导数曲线为斜率为“1/2”的平行直线;⑤第一径向流,此时内区以径向流形式向压裂裂缝及井内流动;⑥第一过渡流,此时中间区向内区流动,由于中间区流度小于内区流度,试井曲线出现抬升;⑦第二径向流,流体在中间区径向流动,压力导数曲线为一条水平线,其数值为 $0.5 M_{12}$;⑧第二过渡流,最外区向中间区流动,由于最外区流度小于中间区流度,试井曲线出现抬升;⑨第三径向流,流体在最外区径向流动,压力导数曲线为一条水平线,其数值为 $0.5 M_{12} * M_{23}$ 。

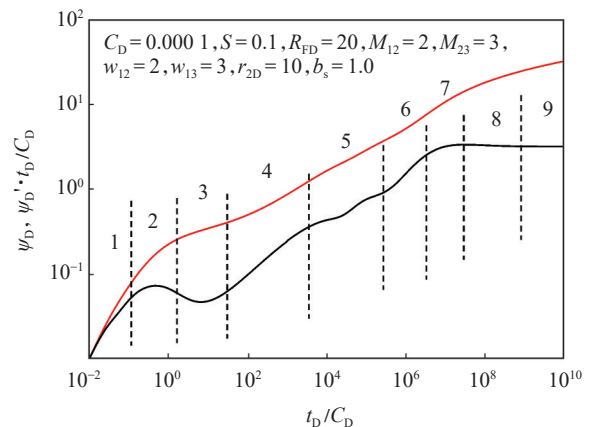


图 3 试井典型曲线

Fig. 3 Type curve of pressure transient

3 参数敏感性分析

3.1 裂缝导流能力的影响

裂缝导流能力作为水力裂缝的重要指标,由水力裂缝的渗透率及水力裂缝宽度决定,水力压裂过程中的压裂液及支撑剂都会对其造成巨大影响。从图4可以看出,裂缝导流能力主要对双线性流及线性流阶段产生影响,裂缝导流能力越大,压力及压力导数越小,双线性流阶段越不明显,导流能力达到一定程度,双线性流消失,试井曲线变为无限导流能力试井曲线。裂缝导流能力越强,CO₂越容易注入,能够更好地对低渗透油藏进行开发。

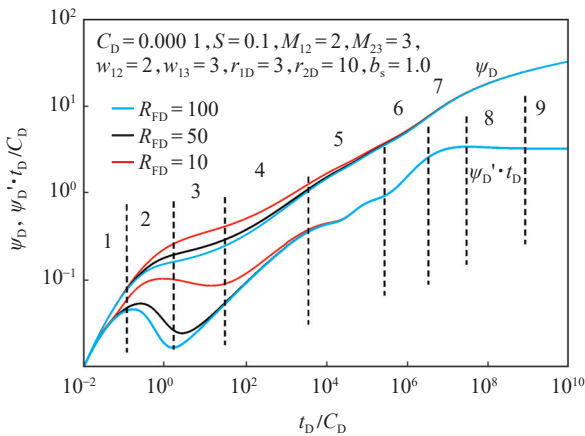


图4 裂缝导流能力对试井曲线的影响
Fig. 4 Effect of fracture conductivity on pressure transient type curve

3.2 空间变导流的影响

裂缝导流能力受施工影响,裂缝一般为楔形缝,裂缝导流能力随裂缝的延伸而减小。本文设置空间变导流能力系数 b_s 为 0, 0.8, 1.0 等 3 组数据,裂缝空间导流能力分布如图5所示。考虑裂缝导

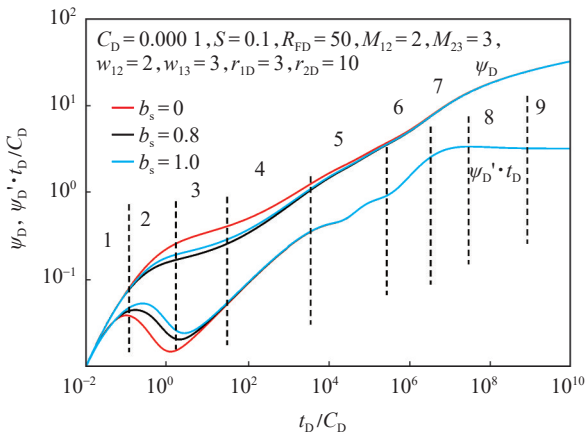


图5 无因次导流能力分布曲线
Fig. 5 Schematic of space variable conductivity of the hydraulic fracture

流能力变化后,从如图6可以看出,早期压差增大,压力及压力导数曲线都呈现一定的上升,表现出表皮系数增大的现象。不考虑裂缝导流能力的空间变化会对试井解释造成较大影响。

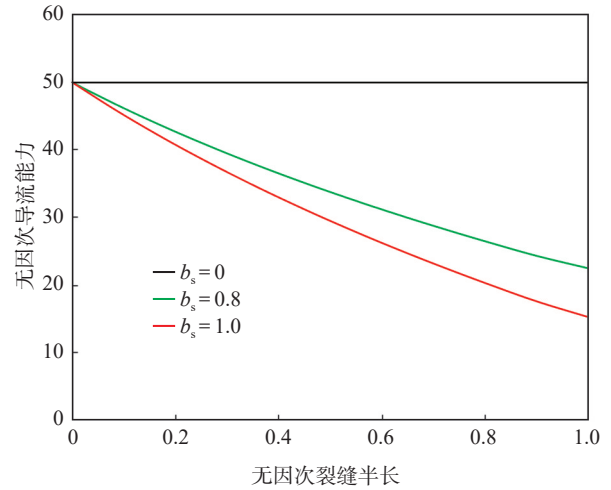


图6 空间变导流系数对试井曲线的影响
Fig. 6 Effect of space variable conductivity on pressure transient type curve

3.3 一区半径的影响

随着注入CO₂的不断增加,CO₂区半径会不断增大。设置不同的CO₂区无因次半径,试井曲线如图7所示,内区半径主要对内区径向流和过渡段产生影响,内区半径越小,过渡流出现的时间越早,内区径向流持续时间越短,内区半径过小时,内区径向流将会被掩盖。

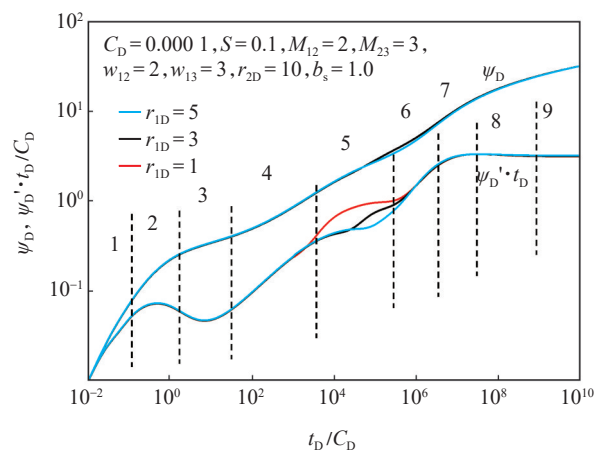


图7 CO₂区半径对试井曲线的影响
Fig. 7 Effect of r_{1D} on rate transient type curve

3.4 二区半径的影响

CO₂注入量、扩散系数及原油的物性特征都会对过渡区的半径产生较大影响。设置不同的过渡区无因次半径,试井曲线如图8所示,过渡区半径

主要对第二径向流和过渡段阶段产生影响,过渡区半径越小,第二过渡流出现的时间越早,第二径向流持续时间越短,过渡区半径过小时,第二径向流将会被掩盖。

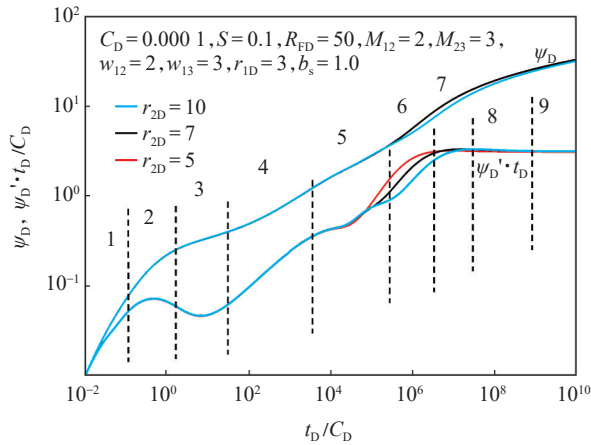


图 8 过渡区半径对试井曲线的影响
Fig. 8 Effect of r_{2D} on rate transient type curve

3.5 CO₂ 与过渡区流度比 M_{12} 的影响

流度是影响流动和压力波传播的重要因素,过渡区为油气混合区,其流度小于内区纯气相流度。设置不同的内区与过渡区流度比,试井曲线如图 9 所示,从图中可以看出,内区与过渡区流度比主要对过渡区及最外区流动阶段产生影响,内区与过渡区流度比越大,则表示过渡区流度越小,其流动阻力较大,则过渡区及最外区流动阶段所消耗的压差越大,因此过渡区及最外区流动阶段压力及压力导数曲线都会抬升。

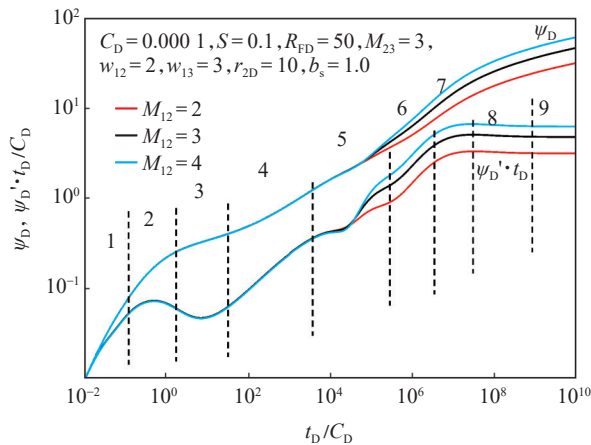


图 9 过渡区与原油区流度比对试井曲线的影响
Fig. 9 Effect of mobility ratio M_{23} on rate transient type curve

3.6 过渡区与原油区流度比 M_{23} 的影响

过渡区为油气混合区,最外区为纯油相流动,

最外区流度小于过渡区流度。设置不同的过渡区与最外区流度比,试井曲线如图 10 所示,过渡区与最外区流度比主要对最外区流动阶段产生影响,过渡区与最外区流度比越大,则表示对应的最外区流动越小,最外区流动阻力越大,最外区流动阶段所消耗的压差越大,因此最外区流动阶段压力及压力导数曲线都会抬升。

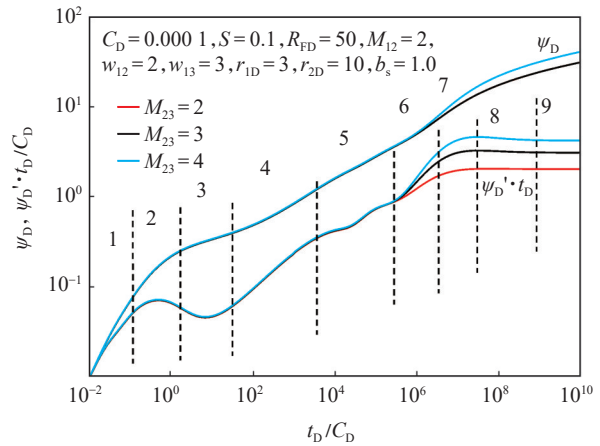


图 10 CO₂ 与过渡区流度比对试井曲线的影响
Fig. 10 Effect of mobility ratio M_{12} on rate transient type curve

4 结论

(1) 利用 Laplace 变换对 CO₂ 三区复合空间变导流能力压裂直井解析解进行了推导,利用 Stehfest 数值反演绘制试井典型曲线。典型曲线可分为井筒储集段、井筒储集后过渡段、双线性流段、地层线性流段、第一径向流段、第一过渡流段、第二径向流段、第二过渡流段、第三径向流段共 9 个阶段。

(2) 裂缝导流能力越大,双线性流阶段压力及压力导数越小,双线性流阶段越不明显,导流能力达到一定程度,双线性流消失,试井曲线变为无限导流能力试井曲线。裂缝导流能力受施工影响,裂缝一般为楔形缝,考虑裂缝导流能力变化后,早期压差增大,压力及压力导数曲线都呈现一定的上升,表现出表皮系数增大的现象。

(3) CO₂ 半径越小,第一过渡流阶段出现的时间越早,内区径向流持续时间越短;过渡区半径越小,第一过渡流阶段出现的时间越早,第二径向流持续的时间越短。

(4) 内区与过渡区流度比越大,则过渡区及最外区流动阶段所消耗的压差越大,因此过渡区及最外区流动阶段压力及压力导数曲线都会抬升;过渡区与最外区流度比越大最外区流动阶段所消耗的

压差越大,最外区流动阶段压力及压力导数曲线都会拾升。

参考文献:

- [1] 胡文瑞,魏漪,鲍敬伟. 中国低渗透油气藏开发理论与技术进展. 石油勘探与开发,2018,45(4):646-656.
HU W R, WEI Y, BAO J W. Development of the theory and technology for low permeability reservoirs in China. Petroleum Exploration and Development, 2018, 45(4): 646-656.
- [2] 袁士义,王强. 中国油田开发主体技术新进展与展望. 石油勘探与开发,2018,45(4):657-668.
YUAN S Y, WANG Q. New progress and prospect of oilfields development technologies in China. Petroleum Exploration and Development, 2018, 45(4): 657-668.
- [3] 唐梅荣,张同伍,白晓虎,等. 孔喉结构对 CO₂ 驱储层伤害程度的影响. 岩性油气藏,2019,31(3):113-119.
TANG M R, ZHANG T W, BAI X H, et al. Influence of pore throat structure on reservoir damage with CO₂ flooding. Lithologic Reservoirs, 2019, 31(3): 113-119.
- [4] 杨红,王宏,南宇峰,等. 油藏 CO₂ 驱油提高采收率适宜性评价. 岩性油气藏,2017,29(3):140-146.
YANG H, WANG H, NAN Y F, et al. Suitability evaluation of enhanced oil recovery by CO₂ flooding. Lithologic Reservoirs, 2017, 29(3): 140-146.
- [5] TANG R W, AMBASTHA A K. Analysis of CO₂ pressure transient data with two-and three-region analytical radial composite models. SPE 18275, 1988.
- [6] SU K, LIAO X, ZHAO X. Transient pressure analysis and interpretation for analytical composite model of CO₂ flooding. Journal of Petroleum Science and Engineering, 2015, 125: 128-135.
- [7] 阎燕,李友全,于伟杰,等. 低渗透油藏 CO₂ 驱采油井试井模型. 断块油气田,2018,25(1):80-84.
YAN Y, LI Y Q, YU W J, et al. Well test model research for CO₂ flooding production well in low permeability reservoirs. Fault-Block Oil & Gas Field, 2018, 25(1): 80-84.
- [8] 李友全,韩秀虹,阎燕,等. 低渗透油藏 CO₂ 吞吐压力响应曲线分析. 岩性油气藏,2017,29(6):122-130.
LI Y Q, HAN X H, YAN Y, et al. Pressure transient analysis on CO₂ huff and puff in low permeability reservoir. Lithologic Reservoirs, 2017, 29(6): 122-130.
- [9] 苏玉亮,孟凡坤,周诗雨,等. 低渗透油藏 CO₂ 驱试井曲线特征分析. 科技导报,2015,33(18):34-39.
SU Y L, MENG F K, ZHOU S Y, et al. Characteristics analysis of well testing curve of CO₂ flooding in low permeability reservoir. Science & Technology Review, 2015, 33(18): 34-39.
- [10] LI L, VOSKOV D V, YAO J, et al. Multiphase transient analysis for monitoring of CO₂ flooding. Journal of Petroleum Science and Engineering, 2018, 160: 537-554.
- [11] LI L, YAO J, LI Y, et al. Pressure-transient analysis of CO₂ flooding based on a compositional method. Journal of Natural Gas Science and Engineering, 2016, 33: 30-36.
- [12] 姜瑞忠,张海涛,张伟,等. CO₂ 驱三区复合油藏水平井压力动态分析. 油气地质与采收率,2018(6):63-70.
JIANG R Z, ZHANG H T, ZHANG W, et al. Dynamic pressure analysis of three-zone composite horizontal well in oil reservoirs for CO₂ flooding. Petroleum Geology and Recovery Efficiency, 2018(6): 63-70.
- [13] TENG W C, QIAO X, TENG L, et al. Production performance analysis of multiple fractured horizontal wells with finite-conductivity fractures in shale gas reservoirs. Journal of Natural Gas Science and Engineering, 2016, 36: 747-759.
- [14] GUO J, WANG H, ZHANG L. Transient pressure and production dynamics of multi-stage fractured horizontal wells in shale gas reservoirs with stimulated reservoir volume. Journal of Natural Gas Science & Engineering, 2016, 35: 425-443.
- [15] 姬靖皓,席家辉,曾凤凰,等. 致密油藏分段多簇压裂水平井非稳态产能模型. 岩性油气藏,2019,31(4):157-164.
JI J H, XI J H, ZENG F H, et al. Unsteady productivity model of segmented multi-cluster fractured horizontal wells in tight oil reservoir. Lithologic Reservoirs, 2019, 31(4): 157-164.
- [16] JIA P, CHENG L S, HUANG S J, et al. Pressure-transient analysis of a finite-conductivity inclined fracture connected to a slanted wellbore. SPE Journal, 2016, 21(2): 522-537.
- [17] 郭建春,路千里,曾凡辉. 楔形裂缝压裂井产量预测模型. 石油学报,2013,34(2):346-352.
GUO J C, LU Q L, ZENG F H. A productivity prediction model for a fractured well with wedge-shaped fractures. Acta Petrolei Sinica, 2013, 34(2): 346-352.
- [18] 孙贺东,欧阳伟平,张冕,等. 考虑裂缝变导流能力的致密气井现代产量递减分析. 石油勘探与开发,2018,45(3):98-106.
SUN H D, OUYANG W P, ZHANG M, et al. Advanced production decline analysis of tight gas wells with variable fracture conductivity. Petroleum Exploration and Development, 2018, 45(3): 98-106.
- [19] 高阳,赵超,董平川,等. 致密气藏变导流能力裂缝压裂水平井不稳定渗流模型. 大庆石油地质与开发,2015,34(6):141-147.
GAO Y, ZHAO C, DONG P C, et al. Transient flow model of the fractured horizontal well with variable conductivity fractures in tight gas reservoirs. Petroleum Geology and Oilfield Development in Daqing, 2015, 34(6): 141-147.
- [20] LUO W J, TANG C F. A semianalytical solution of a vertical fractured well with varying conductivity under non-Darcy-flow condition. SPE Journal, 2015, 20(5): 1028-1040.
- [21] HUANG Y, CHENG S Q, YU H Y, et al. A semianalytical approach to estimate fracture closure and formation damage of vertically fractured wells in tight gas reservoir. Journal of Petroleum Science and Engineering, 2017, 150: 85-90.
- [22] LIU Q L, TIAN S C, YU W, et al. A semi-analytical model for simulation of fluid flow in tight rock with irregular fracture geometry. Journal of Petroleum Science and Engineering, 2019, 174: 14-24.
- [23] LIU J, LIU P C, LI S M, et al. A mathematical model and semi-analytical solution for transient pressure of vertical fracture with varying conductivity in three crossflow rectangular layers. Energy Exploration and Exploitation, 2019, 37(1): 230-250.

(编辑:吕锡敏)